Journal of Natural Resource Conservation and Management
Vol. 6, No. 2, pp 203-213, 2025
doi: 10.51396/ANRCM.6.2.2025.203-213

Land use and land cover change dynamics in Solan district of Himachal Pradesh using geospatial techniques

Nandini Narula[1,*], Arun Kaushal[1], Harpinder Singh[2], and Preeti[1]

[1]Department of Soil and Water Engineering, Punjab Agricultural University, Ludhiana-141004, Punjab, India
[2]Punjab Remote Sensing Centre, Ludhiana-141004, Punjab, India
**Corresponding author email: nandininarula3@gmail.com*

Received : October 22, 2025
Revised : December 06, 2025
Accepted : December 11, 2025
Published : December 31, 2025

ABSTRACT

Land Use and Land Cover (LULC) change analysis plays a vital role in understanding landscape dynamics and the impacts of human activities on the environment, especially in ecologically sensitive mountainous regions. This study examines the spatial and temporal variations in LULC in Solan district of Himachal Pradesh using artificial intelligence and geospatial approaches for the period 2018 to 2025. The main objectives were to prepare reliable LULC maps and to assess changes in LULC patterns. Sentinel-2 satellite data was processed using the cloud-based Google Earth Engine (GEE) platform. Supervised classification was carried out using the Random Forest algorithm. The study area (1936 km^2) was categorized into five LULC classes: agriculture, built-up, water bodies, barren land, and forest. The results revealed notable changes in LULC during the study period. In 2018, forest land constituted the largest share of the area (57.50%), followed by barren land (19.44%), agriculture (12.65%), built-up areas (8.34%), and water bodies (2.07%). By 2025, built-up areas expanded substantially to 13.35%, indicating rapid urban growth. In contrast, agricultural land and water bodies declined to 12.12% and 0.63%, respectively, while barren land decreased to 14.16%. Forest cover increased to 59.71%, suggesting vegetation recovery and afforestation in certain regions. The classification results were highly reliable, with overall accuracies of 90.4% for 2018 and 92.0% for 2025 and corresponding kappa coefficient values of 0.87 and 0.89.

Keywords: Geospatial, Google earth engine, Land use and land cover, Random Forest algorithm, Solan

INTRODUCTION

Land use and land cover are two closely associated terms that are often used together but represent distinct concepts. Land cover refers to the physical and biological characteristics of the Earth's surface, such as forests, water bodies, agricultural land, barren areas and built-up regions, whereas land use describes the manner in which humans utilize land for socio-economic purposes including agriculture, urban development, industrial activities and conservation. The distinction between land use and land cover is important, as land cover represents the biophysical state of the land, while land use reflects human interventions and management practices (Digra and Kaushal, 2021; Khalid *et al.*, 2024). Changes in LULC are driven by a complex interaction of anthropogenic and natural factors. Rapid urbanization, agricultural expansion and industrialization are among the dominant human-induced drivers, while climate change, natural disasters, floods, wildfires and earthquakes also play a significant role by altering vegetation patterns and land surface characteristics (Bhardwaj *et al.*, 2019; Abbas *et al.*, 2025; Muhammad *et al.*, 2022).

Monitoring and assessment of LULC change are essential for understanding landscape dynamics, environmental degradation and sustainable resource management. Geospatial technologies have emerged

as powerful tools for LULC studies, offering efficient means to collect, process, analyse and visualize spatial data. These technologies include Geographic Information Systems (GIS) for spatial analysis and mapping, the Global Positioning System (GPS) for accurate location data and remote sensing, which enables systematic observation of the Earth's surface using satellite or airborne sensors (Amgoth *et al.*, 2023; Hanafi *et al.*, 2024). Among these, remote sensing and GIS are the most widely applied tools for LULC mapping and change detection. Satellite platforms such as Landsat, MODIS and Sentinel-2 provide consistent, repetitive and long-term datasets that allow researchers to monitor deforestation, urban expansion, agricultural transformation and other land surface changes at multiple spatial and temporal scales (Alshari *et al.*, 2023; Sharma *et al.*, 2023).

The increasing availability of cloud-based geospatial platforms has further strengthened LULC research. Google Earth Engine is a cloud-based geospatial analysis platform that enables large-scale analysis of satellite imagery and is particularly valuable for studies related to land use and land cover change, climate change, urbanization, deforestation and natural hazards (Huang *et al.*, 2017; Singh *et al.*, 2021). One of the major strengths of GEE is its extensive data repository, which includes multi-decadal satellite datasets from Landsat, Sentinel, MODIS and other missions, providing global coverage for long-term environmental monitoring. The GEE code editor, based on JavaScript, offers an accessible environment for users with varying programming expertise and supports diverse geospatial operations such as image pre-processing, spectral index computation and machine learning-based classification through integration with the Earth Engine application programming interface (API) (Chen *et al.*, 2023).

Despite significant technological advancements, accurate generation and prediction of LULC maps remain challenging due to the complex interactions among socio-economic factors, environmental conditions and policy influences, particularly under increasing population pressure. In recent years, artificial intelligence (AI) and machine learning (ML) techniques have revolutionized LULC analysis by providing more accurate, efficient and scalable approaches. Land cover classification has emerged as one of the most extensively developed application domains using GEE integrated with AI methods (Lemenkova, 2024; Yang *et al.*, 2022). Machine learning algorithms such as classification and regression trees (CART), random forest (RF), k-nearest neighbours (KNN) and support vector machine (SVM) are widely used for high-accuracy LULC classification using satellite imagery. Continuous advancements in Earth observation technologies, coupled with cloud computing, have enabled large-scale, time-series LULC mapping on GEE by efficiently processing vast volumes of satellite data (Ahmed *et al.*, 2024). Among the available ML techniques, supervised classification using the RF algorithm has gained particular importance due to its robustness, ability to handle high-dimensional datasets and superior classification performance. Supervised classification involves training a model using reference samples that link spectral information from satellite images with known land cover classes derived from ground truth data (Abijith and Saravanan, 2021). The strong integration of AI-based classifiers within the GEE environment, especially the widespread use of RF algorithms, has made this approach increasingly popular for addressing diverse geospatial and environmental problems (Nasiri *et al.*, 2022; Yang *et al.*, 2022).

Although numerous studies have successfully applied AI and geospatial techniques for LULC analysis at regional, national and global scales, comprehensive studies focusing on the Solan district of Himachal Pradesh remain limited. Given the region's rapid development, complex terrain and ecological sensitivity, understanding recent LULC dynamics is essential for sustainable land-use planning and environmental management. Therefore, the present study was undertaken with the objectives to generate LULC change maps of the study area and to evaluate LULC changes over the period from 2018-2025 using artificial intelligence and geospatial methodologies.

MATERIALS AND METHODS

Study Area

The present study area, Solan district (Fig. 1), is situated in southern Himachal Pradesh (India), about 46 km south of Shimla, between 30.05°-31.15° N latitude and 76.42°-77.20° E longitude. Lying at an average elevation of about 1,600 m above mean sea level, the district experiences a temperate climate

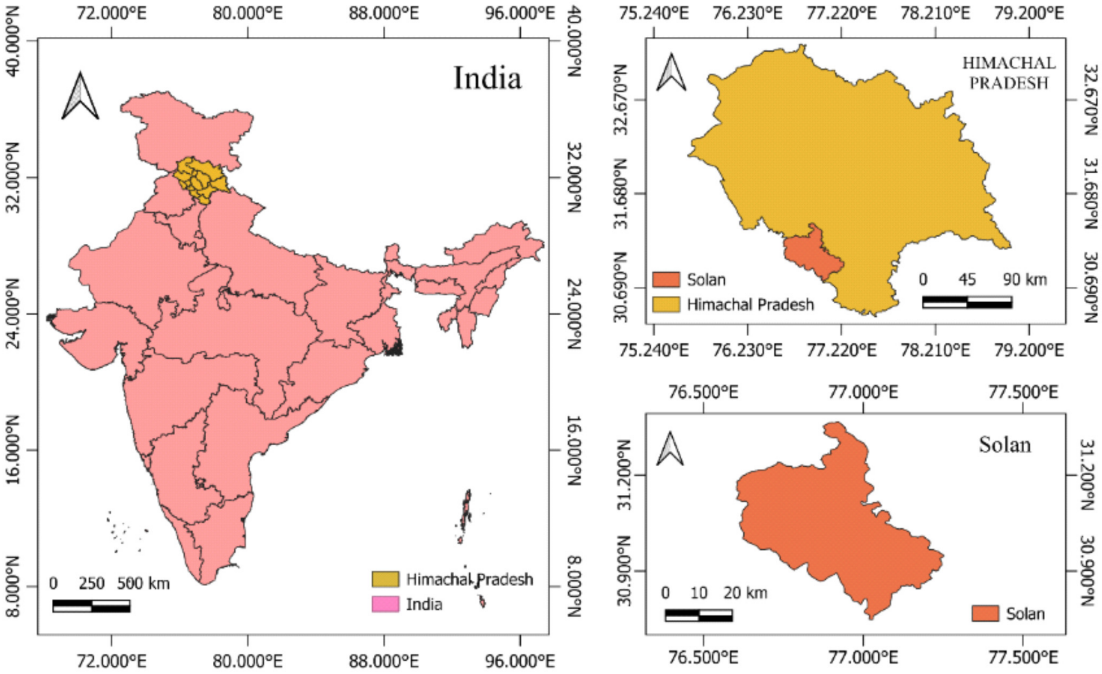

Fig. 1. Location map of study area

favorable for diverse agricultural activities (Anonymous, 2025a). Solan is bounded by Shimla, Sirmaur, Bilaspur, Ropar (Punjab) and Ambala (Haryana) districts. Solan district covers a geographical area of 1,936 km², accounting for 3.49% of the total area of Himachal Pradesh. The district is popularly known as the "Mushroom city of India" and is predominantly mountainous, with the Nalagarh valley forming a relatively flat tract. Agriculture remains the primary livelihood, with Solan being well known for off-season vegetables, mushroom cultivation, and emerging industrial and educational activities (Anonymous, 2025b).

Data Collection

This study used multispectral Sentinel-2A satellite data from the ESA Copernicus programme. Sentinel-2A provides high-resolution imagery across visible to shortwave infrared bands, suitable for LULC mapping. ALOS PALSAR-1 DEM data was used for slope and elevation estimation of the study area.

Software Used

GEE a cloud-based geospatial processing platform was used to analyze and visualize large-scale earth observation data using satellite imagery and geospatial datasets, desktop QGIS software (3.42) was used for spatial analysis and map preparation while, Microsoft office suite was used for data tabulation, calculations and documentation.

Composite Image Preparation

Sentinel-2 images of June and February for 2018 and 2025 covering Solan district were processed in GEE. Images were filtered by study area, acquisition date, and cloud cover, and only scenes with less than 5% cloud contamination were selected. Spectral indices (Table 1) were generated and stacked with the original bands to enhance LULC judgement.

Table 1. Spectral indices

S. No.	Index	Detail	Application
1	NDVI	Normalized Difference Vegetative Index	Vegetation's photosynthetic activity (greenness)
2	NDBI	Normalized Difference Built-up Index	Automatically mapping urban areas
3	MNDWI	Modified Normalized Difference Water Index	Enhancing water bodies
4	BSI	Bare Soil Index	Enhancing bare soil areas, fallow lands

Elevation and slope layers derived from the ALOS PALSAR dataset were also added to the stack. Seasonal composites for June and February of each year were generated and then merged to produce annual combined false color composites (Fig. 2-3) comprising 23 bands. This methodology follows the approach suggested by Nasiri *et al.,* (2022).

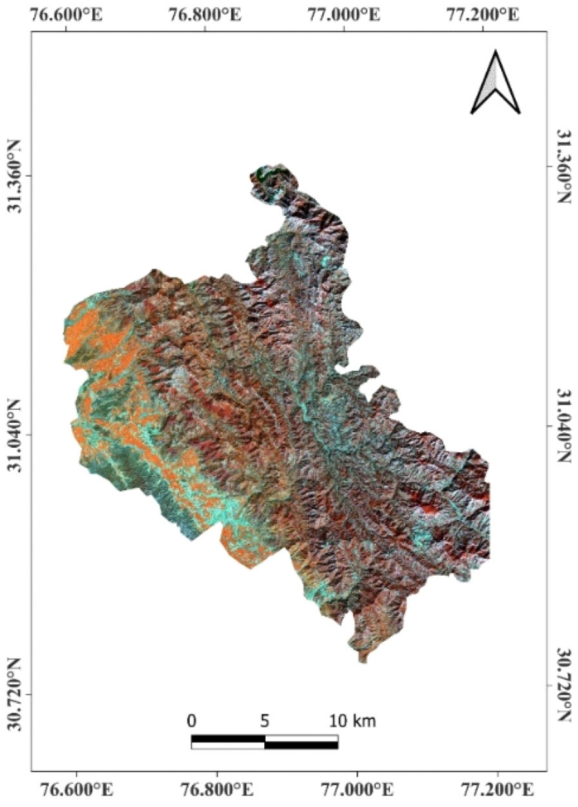

Fig. 2. Combined false color composite (2018)

Land Use Land Cover Classification

Land use and land cover classification of Solan district was carried out by defining five classes: agriculture, built-up, water, barren and forest (Table 2). Training samples for each class were uniformly distributed across the study area using Sentinel-2 imagery, local knowledge, and high-resolution GEE

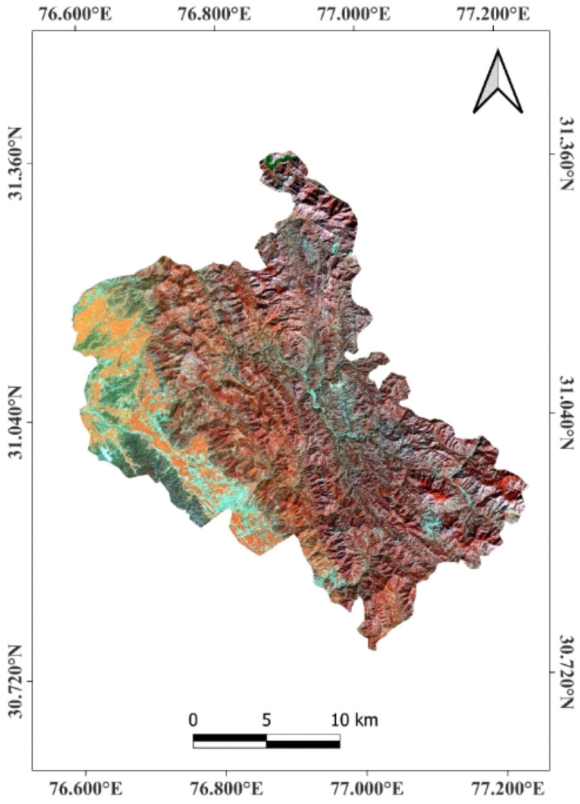

Fig. 3. Combined false color composite (2025)

visuals. A total of 339 reference points for 2018 and 379 for 2025 were generated and divided into training (70%) and validation (30%) datasets (Table 3). The classification was performed in GEE using the RF algorithm, a robust supervised machine learning method widely applied in remote sensing. RF was trained using multispectral Sentinel-2 bands and derived indices to learn the spectral characteristics of each land cover class. The algorithm constructs multiple decision trees using random subsets of training samples and features, and final class assignment for each pixel was based on majority voting. The trained model was applied to the image composites to produce pixel-wise LULC

Table 2. Land use land cover classes of Solan district

Sr. No.	Classes	Description
1	Agriculture	Agricultural land
2	Built-up	Urban and rural settlements
3	Water	Natural and artificial waterbodies like rivers, canals
4	Barren	Cultivable waste, barren, mining and fallow
5	Forest	Forest, shrub, pastures

Table 3. Number of training points for land use land cover classification of Solan district

Classes	Training points	
	2018	2025
Cropland	77	84
Built-up	87	96
Water	45	55
Barren	61	81
Forest	69	63
Total	339	379

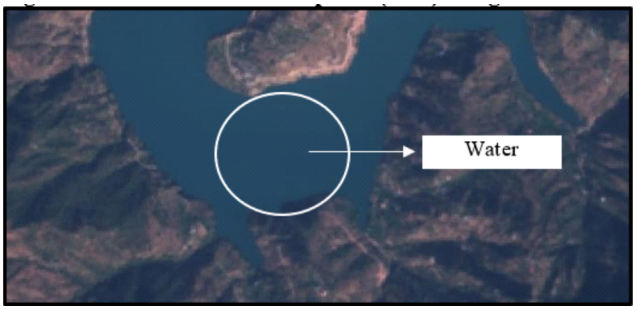

Fig. 4. Water class at latitude 76°52′40″, longitude 31°21′5″

Fig. 5. Agriculture class at latitude 76°40′54″, longitude 31°01′51″

maps. Subsequently, class-wise area statistics were computed, and the final LULC maps were exported in GeoTIFF format. Ground verification is an essential step in remote sensing studies to assess the reliability and accuracy of LULC classifications derived from satellite data. It ensures that mapped classes accurately represent real ground conditions. In this study, ground verification was carried out using the GEE platform (Fig. 4-5). Representative validation points corresponding to different LULC classes from the 2018 classification map were selected. These points were verified using high-resolution Sentinel-2 imagery available in GEE through visual interpretation of spectral and spatial characteristics. The comparison confirmed consistency between the classified LULC categories and observed ground features, demonstrating the reliability of the classification results.

Accuracy Assessment

Accuracy assessment of land use land cover classification in GEE involves comparing the classified map with reference data to evaluate its reliability. A confusion matrix of test samples was generated to get the overall accuracy (OA), producer accuracy (PA), user accuracy (UA) and kappa coefficient (κ). These were computed by using equations 1 to 4.

$$\text{Overall accuracy} = \frac{\text{Number of correctly classified points (Diagonal)}}{\text{Total number of reference points}} \quad \ldots (1)$$

$$\text{Producer accuracy} = \frac{\text{Number of correctly classified points in each category}}{\text{Total number of reference points in that category (The column total)}} \quad \ldots(2)$$

$$\text{User's accuracy} = \frac{\text{Number of correctly classified points in each category}}{\text{Total number of reference points in that category (the row total)}} \quad \ldots(3)$$

$$\text{Kappa coefficient} = \frac{(po - pe)}{1 - pe} \quad \ldots(4)$$

Where p_o is the proportion of observed agreements and p_e is the proportion of agreements expected by chance (Saputra and Lee, 2019).

Land Use Land Cover Change Analysis

LULC maps for the year 2018 and 2025 were first exported to google drive in GeoTiff format and merged together in such a way that one layer lay above another. A transitional map was generated further to observe the changes occurred between this period. It provided detail insights into how LULC classes have evolved over the years. Each value in the matrix represented the area that transitioned from one LULC category to another. This transition not only reflects natural changes but also anthropogenic influences such as urban expansion, deforestation, and land degradation or reclamation.

RESULTS AND DISCUSSIONS

Land Use Land Cover Classification Maps of 2018 and 2025 for Solan District

The LULC classification maps for 2018 (Fig. 6) and 2025 (Fig. 7) illustrate the spatial distribution of five land cover classes across Solan district. Forest cover dominated the landscape, followed by barren land and agricultural areas, while built-up areas and water bodies occupied comparatively smaller extents. Agricultural land was mainly concentrated in low-lying and gently sloping regions, whereas built-up areas were clustered around urban and semi-urban settlements. Barren land largely represented rocky terrain, fallow land and mining-affected areas.

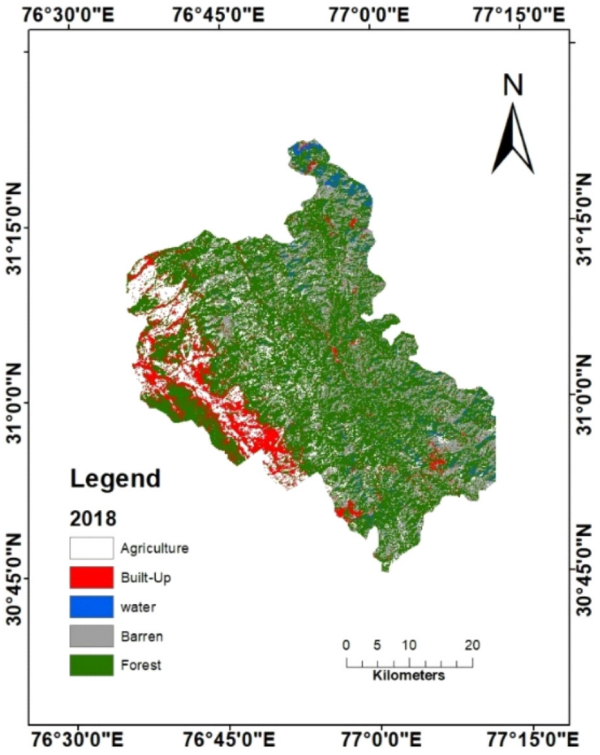

Fig. 6. LULC classification map (2018)

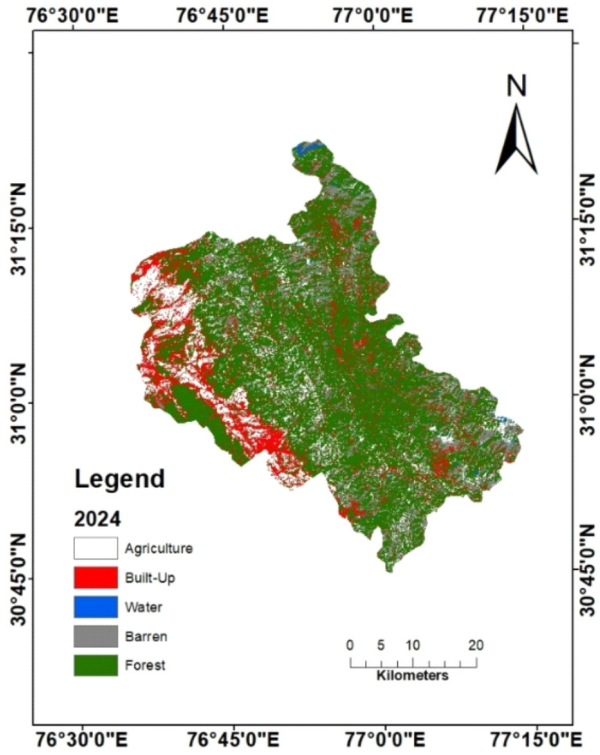

Fig. 7. LULC classification map (2025)

Table 4. LULC classification (2018)

S.No.	LULC classes	Area (km²)	Area (%)
1	Agriculture	244.97	12.65
2	Built-up	161.53	8.34
3	Water	40.03	2.07
4	Barren	376.45	19.44
5	Forest	1113.17	57.50

Table 5. LULC classification (2025)

S. No.	LULC classes	Area (km²)	Area (%)
1	Agriculture	234.76	12.12%
2	Built-up	258.60	13.35%
3	Water	12.31	0.63%
4	Barren	274.26	14.16%
5	Forest	1156.05	59.71%

The LULC distribution for 2018 (Table 4) indicates forest as the dominant land cover, accounting for about 57.50% of the district area (1113.17 km²), followed by barren land covering 376.45 km² (19.44%). Agricultural land extends over 244.97 km², contributing 12.65% to the total area, while built-up areas cover 161.53 km² (8.34%). Water bodies occupy the smallest area, spanning only 40.03 km², which accounts for 2.07% of the total geographical area. Similarly, the LULC distribution for 2025 (Table 5) shows forest as the predominant land cover, accounting for about 59.71% of the district area (1156.05 km²), emphasising the ecological significance of the region. Barren land declined to 274.26 km² (14.16%), while agricultural land covered 234.76 km², accounting for 12.12% of the district area. In contrast, built-up areas expanded significantly, occupying 258.60 km² (13.35%), reflecting increasing urbanization. Water bodies showed a notable decline, covering only 12.31 km², which represents approximately 0.63% of the total area.

The observed increase in forest cover between 2018 and 2025 may be attributed to afforestation initiatives, natural regeneration and stricter forest conservation policies implemented in the Himalayan region, as also reported in similar mountainous landscapes by Huang *et al.*, (2017) and Khalid *et al.*, (2024). The decline in barren land suggests a gradual transition of fallow and degraded areas into forest or built-up categories, a trend commonly associated with land reclamation and infrastructure development (Nasiri *et al.,* 2022; Baghel *et al.,* 2024). The substantial expansion of built-up areas highlights

the growing influence of population pressure, tourism and urban sprawl in Solan district, consistent with findings from other Indian and Himalayan regions using GEE and machine learning approaches (Singh *et al.,* 2021; Rana *et al.,* 2022; Abbas *et al.,* 2025). The sharp reduction in water bodies is a matter of concern and may be linked to climate variability, reduced precipitation and increased anthropogenic water extraction, echoing observations made by Hanafi *et al.,* (2024), emphasizing the need for sustainable land and water resource management.

Accuracy Assessment

Accuracy assessment was performed using confusion matrices generated from independent validation datasets. The overall accuracy and kappa coefficients for study period indicate a strong agreement between the classified outputs and reference data, confirming the robustness and reliability of the RF algorithm. For the year 2018, the classification achieved an overall accuracy of 90.4% with a kappa coefficient of 0.87, while for 2025, the overall accuracy further improved to 92.0% with a kappa coefficient of 0.89, reflecting enhanced classification performance and consistency.

In 2018, agriculture exhibited high producer's and user's accuracies of 96.67% and 93.54%, respectively, while water bodies showed balanced accuracies of 90% for both producer's and user's accuracy. Forest class also demonstrated reliable performance with producer's and user's accuracies of 85.7% and 88.8%, Built-up have producer's and user's accuracies of 87.5% and 100%, respectively (Table 6). In 2025, further improvement was observed, particularly for agriculture and forest classes, with agriculture attaining 96% producer's accuracy and 100% user's accuracy, forest achieving 73.91% producer's accuracy and 100% user's accuracy, Built-up have producer's and user's accuracies of 93.54% and 86.11%, respectively, water having the producer's accuracy of 97.74% and user's accuracy of 90%. Minor misclassification was observed between barren land, built-up areas and forest edges, particularly in transitional and heterogeneous zones (Table 7). In 2018, barren land showed relatively lower user's accuracy (73.6%) despite a high producer's accuracy (93.33%), suggesting confusion with built-up and forest fringe areas. Similar patterns were observed in 2025, although improvements were noted, with barren land achieving 100% producer's accuracy and 89.29% user's accuracy, indicating reduced omission errors (Table 7). These misclassifications are largely attributed to spectral similarity and mixed land cover conditions, a common issue in complex mountainous landscapes.

Table 6. Producer's and user's accuracy (2018)

S.No.	LULC classes	Producer's accuracy	User's accuracy
1	Agriculture	96.67	93.54
2	Built-up	87.5	100
3	Water	90	90
4	Barren	93.33	73.6
5	Forest	85.7	88.8

Overall accuracy = 90.4%
Kappa coefficient = 0.87

Table 7. Producer's and user's accuracy (2025)

S.No.	LULC classes	Producer's accuracy	User's accuracy
1	Agriculture	96	100
2	Built-up	93.54	86.11
3	Water	97.74	90
4	Barren	100	89.29
5	Forest	73.91	100

Overall accuracy = 92%
Kappa coefficient = 0.89

The high overall accuracy and kappa coefficients obtained for both 2018 (OA = 90.4%, κ = 0.87) and 2025 (OA = 92.0%, κ = 0.89) confirm the robustness and reliability of the Random Forest classifier for LULC mapping in complex Himalayan terrain. Comparable classification performance has been reported in recent studies using GEE and machine learning, such as Ahmed *et al.* (2024) (OA = 88%, κ = 0.83), Amgoth *et al.* (2023) (OA = 82%, κ = 0.78) and Baghel *et al.* (2024) (κ = 0.79 - 0.88), indicating that the achieved accuracies fall within or exceed the accepted standards for regional-scale LULC studies. The improved class-wise accuracies in 2025, particularly for agriculture (PA = 96%, UA = 100%) and water bodies (PA = 97.74%, UA = 90%), suggest enhanced spectral separability and improved training sample quality over time, as also observed by Singh *et al.* (2021) and Nasiri *et al*. (2022). The relatively lower user's accuracy of barren land in 2018 (UA = 73.6%) and minor confusion at forest, built-up and barren interfaces reflect spectral similarity and mixed pixel effects common in heterogeneous mountainous landscapes, a challenge widely documented in similar studies (Rana *et al.,* 2022; Khalid *et al.,* 2024).

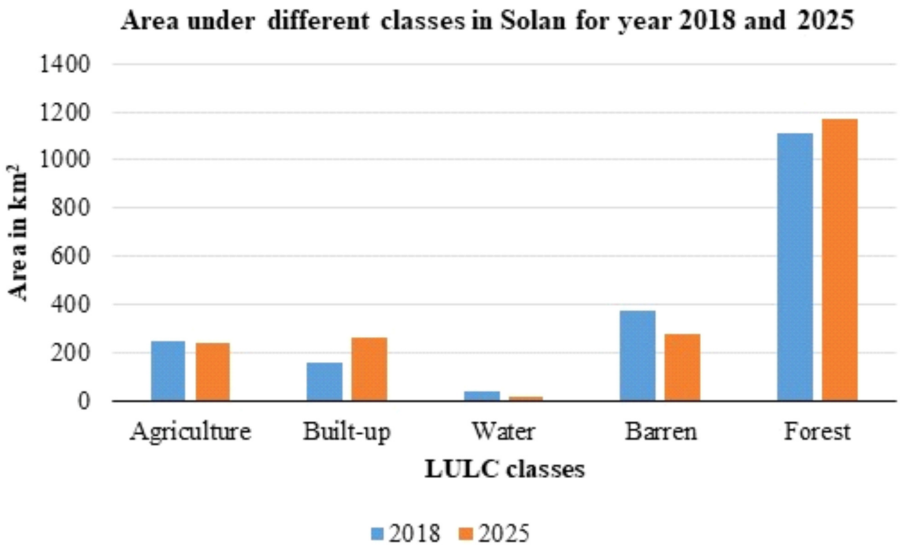

Fig. 8. LULC change in Solan district (2018-25)

Land Use and Land Cover Change Detection of Solan District

The LULC change analysis for Solan district between 2018 and 2025 reveals substantial transitions among the five land cover classes. The most pronounced decrease occurred in barren land by 102.19 km² (5.28%). This was followed by a significant increase in built-up areas, which increased by 97.07 km² (5.01% of total area), indicating rapid urban expansion. Forest cover showed a net increase of 42.88 km² (2.21%), while water bodies declined by 27.72 km² (1.43%). Agricultural land experienced the least change, decreasing by 10.21 km² (0.53%) as shown in Fig. 8. Overall, the results indicate an accelerating urbanization trend with potential environmental implications due to the reduction of natural land cover types, particularly water bodies and barren land as illustrated in LULC transition map (Fig. 9) with its legend details in Table 8. The diverse colour transitions highlighted widespread land cover conversions, largely associated with urban growth and infrastructure development, supporting the observed increase in built-up areas and decline in water and barren land. The transition matrix (Table 9) illustrates class-wise land use/land cover changes between 2018 and 2025. Agricultural land showed moderate stability, retaining 162.10 km². While, notable conversions occurred to forest (35.88 km²), barren land (25.05 km²) and built-up areas (21.58 km²). Built-up maintained an area of 113.70 km² and gaining area primarily from barren land (67.88 km²), forest (55.14 km²) and agriculture (21.58 km²). Water bodies exhibited relatively low stability,

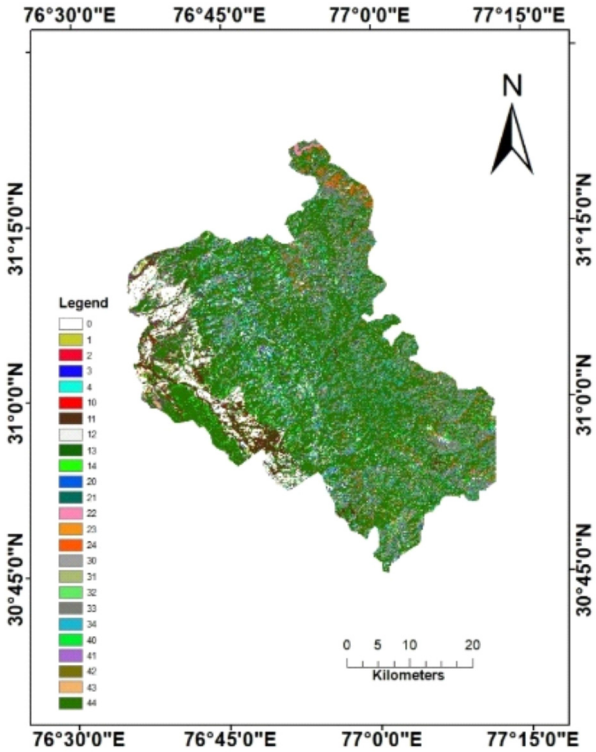

Fig. 9. LULC transition map of Solan district (2018-25)

retaining 6.03 km², with significant conversion to forest (33.95 km²), indicating possible vegetation encroachment or seasonal drying. Barren land retained 185.88 km², but experienced substantial transitions to forest (116.55 km²) and built-up areas (67.88 km²), reflecting both ecological recovery and anthropogenic pressure. Forest cover remained the most dominant and resilient class, retaining 940.23

Table 8. Legend details of Fig. 9

Legend inputs	Class transition	
	From	To
10	Built-up	Agriculture
11	Built-up	Built-up
12	Built-up	Water
13	Built-up	Barren
14	Built-up	Forest
20	Water	Agriculture
21	Water	Built-up
22	Water	Water
23	Water	Barren
24	Water	Forest
30	Barren	Agriculture
31	Barren	Built-up
32	Barren	Water
33	Barren	Barren
34	Barren	Forest
40	Forest	Agriculture
41	Forest	Built-up
42	Forest	Water
43	Forest	Barren
44	Forest	Forest

Table 9. Transition matrix for LULC of Solan district

		Year 2025					
	LULC classes	Agriculture	Built-up	Water	Barren	Forest	Total
Year 2018	Agriculture	162.1	21.58	0.09	25.05	35.88	244.97
	Built-up	9.36	113.7	0.82	8.21	29.44	161.53
	Water	0.01	0.03	6.03	0.01	33.95	40.03
	Barren	5.82	67.88	0.32	185.88	116.55	376.45
	Forest	57.47	55.14	5.05	55.11	940.23	1113.17
	Total	234.76	258.6	12.31	274.26	1156.05	1936

km², although losses to agriculture (57.47 km²), built-up (55.14 km²) and barren land (55.11 km²) were observed.

The LULC transition analysis for Solan district shows a marked increase in built-up area (+97.07 km²; 5.01%), indicating rapid urban expansion, which is comparable to the rise in impervious surfaces reported by Muhammad *et al.,* 2022 (+16.43%) and Kamaraj and Rangarajan, 2022 (+10 km² by 2030). The significant reduction in barren land (–102.19 km²; 5.28%) and its conversion into forest (+116.55 km²) and built-up areas (+67.88 km²) aligns with trends observed by Abijith and Saravanan, 2021 (barren land decrease with built-up expansion) and Dousari *et al.,* 2023 (built-up increase of ~11%). Forest cover in the present study remained dominant with high retention (940.23 km²), similar Abijith and Saravanan 2021, who reported forest stability despite localized losses. The decline in water bodies (–27.72 km²; 1.43%) and their transition into forested areas (+33.95 km²) is consistent with findings of Muhammad *et al.,* 2022 (water bodies +0.37% but fragmented) and Hanafi *et al.,* 2024, highlighting climate variability and vegetation encroachment effects.

CONCLUSIONS

This study evaluated land use and land cover dynamics in Solan district, Himachal Pradesh, using artificial intelligence–based geospatial techniques, with supervised classification performed through the Random Forest algorithm. Five major LULC classes-agriculture, built-up areas, forest, barren land and water bodies were mapped for two time periods. Classification accuracy assessment confirmed the robustness of the adopted methodology, with high overall accuracy and strong agreement between classified maps and reference data, demonstrating the suitability of AI-driven approaches for reliable LULC mapping in complex mountainous terrain. The analysis revealed substantial spatial and temporal changes in land use land cover across the district. Forest cover remained the dominant land class and showed an overall increasing trend, indicating vegetation regeneration and effective land management in certain areas. Built-up land expanded noticeably, reflecting ongoing urbanization and infrastructure development, while agricultural land experienced a slight decline. Barren land showed a considerable reduction, partly attributable to its conversion into forest and built-up areas. In contrast, water bodies exhibited a declining trend, highlighting growing stress on surface water resources. Overall, the observed land cover transitions were primarily driven by urban expansion, land-use intensification and localized ecological recovery. The study emphasizes the value

of AI-enabled and cloud-based geospatial platforms for continuous LULC monitoring and provides an important qualitative baseline to support sustainable land-use planning, environmental conservation and policy formulation in Solan district.

ACKNOWLEDGEMENTS

The authors acknowledge the College of Agricultural Engineering, Punjab Agricultural University, Ludhiana, Punjab (India), for providing the necessary facilities, institutional support and a conducive research environment to carry out this study. Sincere thanks are also extended to the Punjab Remote Sensing Centre, Ludhiana, for supplying essential geospatial data and technical assistance required for the successful completion of the research. The authors are thankful to all faculty members and staff who directly or indirectly contributed to this work through their guidance and support.

REFERENCES

Abbas, T., Shoaib, M., Albano, R., Baig, A.I.M., Ali, I., Farid, H.U. and Ali, M.U. (2025). Artificial-intelligence-based investigation on land use and land cover (LULC) changes in response to population growth in South Punjab, Pakistan. *Land*, *14*, 1–34.

Abijith, D. and Saravanan, S. (2021). Assessment of land use and land cover change detection and prediction using remote sensing and CA-Markov in the northern coastal districts of Tamil Nadu, India. *Environmental Science and Pollution Research*, *29*, 86055–86067.

Ahmed, R., Zafor, M. and Trachte, K. (2024). Land use and land cover changes in Cottbus City and Spree–Neisse District, Germany, in the last two decades: A study using remote sensing data and Google Earth Engine. *Remote Sensing*, *16*, 2773.

Alshari, E., Abdulkareem, M. and Gawali, B. (2023). Classification of land use/land cover using artificial intelligence (ANN–RF). *Frontiers in Artificial Intelligence*, *5*, 964279.

Amgoth, A., Rani, H. and Jayakumar, K. (2023). Exploring land use and land cover changes in Pakhal Lake area, Telangana, India using QGIS MOLUSCE plugin. *Spatial Information Research*, *31*, 429–439.

Anonymous (2025a). *Himachal Pradesh GK: Geography of Solan District*. Retrieved January 23, 2025, from https://himstate.in/himachal-pradesh-gk-geography-of-solan-district

Anonymous (2025b). *District Solan, Government of Himachal Pradesh*. Retrieved January 18, 2025, from https://hpsolan.nic.in/

Baghel, S., Kothari, M.K., Tripathi, M.P., Singh, P.K., Bhakar, S.R., Dave, V. and Jain, S.K. (2024). Spatiotemporal land use and land cover change detection and future prediction for the Mand catchment using MOLUSCE tool. *Environmental Earth Sciences*, *83*, 66.

Bhardwaj*, A.K., Mishra, V.K., Singh, A.K., Arora, S., Srivastava, S., Singh, Y.P. and Sharma, D.K. (2019). Soil salinity and land use-land cover interactions with soil carbon in a salt affected irrigation canal command of Indo-Gangetic plain. CATENA, 180, 392-400. https://doi.org/10.1016/j.catena.2019.05.015

Chen, H., Yang, L. and Wu, Q. (2023). Enhancing land cover mapping and monitoring: An interactive and explainable machine learning approach using Google Earth Engine. *Remote Sensing*, *15*, 4585.

Digra, A. and Kaushal, A. (2021). Land use and land cover change analysis using remote sensing and GIS techniques. *Biological Forum – An International Journal*, *13*, 134–138.

Dousari, A., Mishra, A. and Singh, S. (2023). Land use and land cover change detection and urban sprawl prediction for Kuwait metropolitan region using multi-layer perceptron neural networks (MLPNN). *Egyptian Journal of Remote Sensing and Space Science*, *26*, 381–392.

Hanafi, M., Amara, D., Bounar, R., Mayouf, R., Ali, H. and Ouamane, A. (2024). Artificial intelligence and remote sensing for spatiotemporal analysis and prediction of vegetation changes: A case study of El Oued, northeastern Algeria. *Studies in Engineering and Exact Sciences*, *5*, 1–21.

Huang, H., Chen, Y., Clinton, N., Wang, J., Wang, X., Liu, C., Gong, P., Yang, J., Bai, Y., Zheng, Y. and Zhu, Z. (2017). Mapping major land cover dynamics in Beijing using all Landsat images in Google Earth Engine. *Remote Sensing of Environment*, *202*, 166–176.

Kamaraj, M. and Rangarajan, S. (2022). Predicting the future land use and land cover changes for Bhavani Basin, Tamil Nadu, India using QGIS MOLUSCE plugin. *Environmental Science and Pollution Research*, *29*, 86337–86348.

Khalid, W., Shamim, S. and Ahmad, A. (2024). Synergistic approach for land use and land cover dynamics prediction in Uttarakhand using cellular automata and artificial neural network. *Geomatica*, *76*, 100017.

Lemenkova, P. (2024). Artificial intelligence for computational remote sensing: Quantifying patterns of land cover types around Cheetham Wetlands,

Port Phillip Bay, Australia. *Journal of Marine Science and Engineering*, *12*, 1279.

Muhammad, R., Zhang, W., Abbas, Z., Guo, F. and Gwiazdzinski, L. (2022). Spatiotemporal change analysis and prediction of future land use and land cover changes using QGIS MOLUSCE plugin and remote sensing big data: A case study of Linyi, China. *Land*, *11*, 419.

Nasiri, V., Deljouei, A., Moradi, H., Sadeghi, S.H. and Borz, S.A. (2022). Land use and land cover mapping using Sentinel-2 and Landsat-8 satellite images and Google Earth Engine: A comparison of two composition methods. *Remote Sensing*, *14*, 1977.

Rana, D., Kumari, M. and Kumari, R. (2022). Land use and land coverage analysis with Google Earth Engine and change detection in the Sonipat district of Haryana state, India. *Engineering Proceedings*, *4*, x. https://doi.org/10.3390/xxxxx

Saputra, M. and Lee, H. (2019). Prediction of land use and land cover changes for North Sumatra, Indonesia using an artificial neural network-based cellular automaton. *Sustainability*, *11*, 3024.

Sharma, N., Kaushal, A. and Yousuf, A. (2023). Geospatial technology for assessment of soil erosion and prioritization of watersheds using RUSLE model for lower Sutlej sub-basin of Punjab, India. *Environmental Science and Pollution Research*, *30*, 515–531.

Singh, H., Kochhar, A., Litoria, P. and Pateriya, B. (2021). Land cover classification of Punjab state using Sentinel-2 data and machine learning within the Google Earth Engine cloud platform. *Journal of Geomatics*, *15*, 166–173.

Yang, L., Driscol, J., Sarigai, S., Wu, Q., Chen, H. and Lippitt, C. (2022). Google Earth Engine and artificial intelligence (AI): A comprehensive review. *Remote Sensing*, *14*, 3253.